Adaptive Online Optimization of Alarm Thresholds using Multilayer Bayesian Networks and Active Transfer Entropy

Yi Luo[a,b], Bhushan Gopaluni[b], Liang Cao[b], Yongjian Wang[c], Jian Cheng[a,*]

[a]*Research Institute of Mine Big Data, Chinese Institute of Coal Science, Beijing, 100013, China*
[b]*Department of Chemical and Biological Engineering, University of British Columbia, Vancouver, BC, V6T 1Z3, Canada*
[c]*Department of Automation, Southeast University, Jiangsu, 210096, China*

Abstract

Poorly designed alarm thresholds usually lead to significant safety hazards and highly connected industrial processes. Due to the process condition changes, the traditional alarm threshold optimization methods based on historical alarm data lack the ability to adapt the thresholds online, which increases the safety risks for a given process. This paper proposes a Simplified Multilayers Bayesian Network based on Active Transfer Entropy (SMBN-ATE) to achieve adaptive online optimization of alarm threshold. Through SMBN-ATE, an accurate and streamlined alarm propagation network is constructed and then applied to predict the probability of future alarms, optimizing the alarm thresholds at each sample time. Our method has two primary advantages: (1) The constructed alarm propagation network circumvents the false causality problem caused by strong correlation and thus improves the accuracy of the alarm propagation structure. (2) The adaptive online threshold optimization adjusts threshold value in real-time based on the alarming probability and independently optimizes false and missed alarm rates. The experimental results for the micro-seismic data obtained from an actual coal mine indicate the reliability of establishing variable relationships based on Active Transfer Entropy (ATE). Furthermore, the

*Corresponding author
Email address:* `jiancheng@tsinghua.org.cn` (Jian Cheng)

SMBN-ATE shows high effectiveness in the Tennessee Eastman Process (TEP). Consequently, SMBN-ATE optimized the sum of the average false alarm and missing alarm rates for 16 variables from 28.5% and 27.2% to 19.7%, where 28.5% and 27.2% were calculated by the Univariate threshold setting (Uni) and False Alarm Probability and Missing Alarm Probability (FAP-MAP), respectively. It demonstrated the SMBN-ATE method to be remarkably valuable.

1. Introduction

Modern industrial processes, such as chemical, paper pulping, and coal mining, are highly interconnected and complex. To ensure safe operation, they are equipped with hundreds of alarms. However, these alarms are often poorly designed. Izadi [1] reported catastrophic industrial incidents that can at least partially be attributed to poorly designed alarms; many people are injured or lose their lives yearly due to these accidents. This realization has increased interest in the systematic design of alarms [2, 3, 4]. Recent results from this research brought about a significant improvement in the performance of industrial alarm systems. However, in practice, an excessive number of alarms are set out of an abundance of caution, which usually leads to a common phenomenon called alarm flooding. Alarm flooding is a major cause of chemical accidents and is challenging to manage. Two primary factors are responsible for alarm flooding: chattering and false alarms. Both types of alarms are caused by improper design of alarm thresholds. Therefore, it is critical to choose the alarm threshold optimally.

Based on numerous studies by scholars in alarm design and management, Zhu [5] provided a detailed overview and indicated that optimal management of alarms [6], alarm root cause analysis [7, 8], and alarm threshold optimization [9, 10] are three crucial ways to improve industrial alarm systems significantly. The optimal management of alarms would enhance the ability of operators to

2

respond to sudden unexpected alarms. The alarm root cause analysis can locate the root cause of alarm flooding. However, implementing these two methods relies on accurate information about the alarms. The quality of the alarms depends on the thresholds used in designing them.

Optimizing alarm thresholds is a practical approach often used to reduce alarm flooding and provide accurate alarm information. In recent years, many effective threshold optimization approaches have been put forward, which can be divided into offline and online dynamic threshold optimization. Furthermore, offline threshold optimization contains both single variable and multivariate threshold optimization methods.

Single variable threshold optimization methods have been applied to industrial problems with significant improvement. For example, methods based on dead zones and filters [10] are widely used, but these methods are insensitive to small fluctuations and ignore temporary anomalies. In response to the alarm flooding caused by the instability of process variables, Wang [11] and Adnan [12] proposed the alarm delay method to reduce the number of alarms. Afzal [13] proposed a multi-mode delay timer to adapt to complex industrial processes, which is highly restrictive and can be applied to a non-critical process variable. Han [9] proposed a comprehensive approach to optimize false and missed alarm rates and time delay for threshold optimization. In addition, Yang [14] proposed a method to judge the threshold quality using the Receiver Operating Characteristic (ROC) curve. It is essential to point out that even though the single variable threshold optimization method improves the performance of alarm systems, it still cannot effectively solve the problem of alarm flooding.

As for multivariate threshold optimization methods, modern industrial plants have great potential to optimize alarm thresholds based on massive volumes of alarming data obtained from Distributed Control Systems (DCS) [15] and Supervisory Control And Data Acquisition systems (SCADA) [16]. To judge whether the design of the alarm threshold conforms to the actual chemical process, Zhang [17] optimized the multivariable alarm threshold by estimating the kernel density of the alarm sequence. Considering the correlation between nor-

3

mal data and alarm data, Yang [18] proposed a threshold setting method to optimize the alarm threshold based on the corresponding correlation. Based on the distribution characteristics of alarm data, Cheng [19] calculated the data's potential features through manifold learning and provided stable information for threshold setting. Han [9] and Gao [20] presented a method to optimize the alarm threshold for variables in an alarm path by combining the analysis of missed and false alarm rates and the correlation of relevant variables, significantly improving alarm accuracy. Although multivariate threshold optimization techniques have been extensively studied, they are still not robust for complex chemical processes with varying operating conditions because all the parameters are calculated based on offline optimization.

Online dynamic alarm threshold optimization can be accomplished using machine learning and statistical algorithms. Using the historical data of process operations, Bristol [21] optimized the alarm threshold and developed an algorithm to adjust the alarm threshold automatically. Using trend data analysis, Rossum [22] optimized the alarm threshold based on dynamic data analysis. Integrating the Artificial Immune System Fault Diagnosis (AISFD) method [23] and the Bayesian Estimation-based Dynamic Alarm Management (BEDAM) method [24], Zhu [25] proposed an online real-time detection algorithm to reduce the number of alarms by dynamically calculating and correcting alarm thresholds. However, those threshold optimization methods mentioned above optimize the thresholds of variables based on past alarm data, which are generally insensitive for each incoming alarm as the processes change.

An accurate estimate of alarm probability is vital to adaptive online optimization of alarm thresholds. On the one hand, Zhu [25] and Amin [26] studied a dynamic Bayesian Network (BN) inference and prediction approach to estimate the probability of alarms. However, Bayesian Networks need large volumes of data to train parameters, especially in networks with a large number of variables. Since the training of Bayesian Networks requires significant data that may not be available in complex chemical processes, it is challenging to estimate relevant conditional probabilities in complex chemical processes. On the other

4

hand, Meng [27] trained both the BN and Dynamic Bayesian Network (DBN)
structure according to the scoring function calculated by the correlation between
data. However, this approach often leads to incorrect relationships during the
construction of the alarm propagation network. Dai [28] claimed that overcoming false causality relationships and constructing an accurate alarm propagation
network is a challenging problem.

Based on numerous studies by scholars, we put forward an SMBN-ATE
method to obtain an accurate estimate of the alarm propagation network using
unique information propagating between variables first. SMBN-ATE method
also simplifies the traditional DBN and reduces the need for large volumes of
data during the training process. Based on this simplified structure, we consider
each variable's alarming probability and propose an idea for adaptive online optimization of alarm variables. Before an alarm occurs, the threshold of the
possible alarm variables is optimized to achieve dynamic threshold optimization. Furthermore, the SMBN-ATE-based adaptive online threshold optimization minimizes the false alarm rate of each variable's missed alarm rate.

The rest of this paper is summarized as follows. Section 2 provides an
overview of the traditional Bayesian Network training and the primary multivariate alarm threshold optimization method. Section 3 describes the proposed
method SMBN-ATE in detail and introduces the dynamic threshold optimization method based on alarm probability. Section 4 demonstrates the effectiveness of the proposed approach through micro-seismic data obtained from
an actual coal mine process and the Tennessee Eastman process (TEP); these
two experiments show the significance of the adaptive online alarm threshold
optimization method, followed by conclusions in Section 5.

The main highlights of this paper are summarized as follows:

(1) The proposed method simplifies traditional DBN, works with limited data,
and provides alarm propagation probability based on causality analysis.
Compared with ATE, the method proposed in this paper expands the alarm
propagation structure to multiple layers and provides more interpretable

and accurate alarm relations in the time dimension through this structure ₁₁₅ to support the work of adaptive threshold optimization on a small amount of data.

(2) The proposed online optimization method adaptively updates the alarm thresholds as the process conditions change. Using the probability of each alarm and performing dynamic threshold optimization before the alarm ₁₂₀ occurs, we can provide more accurate information to the operators.

2. Bayesian Networks

This section will introduce the traditional multivariate threshold optimization methods [9, 10] and the Bayesian Network training methods [25, 26, 27]. In addition, this section will introduce the block segmentation algorithm. It ₁₂₅ utilizes a priori process knowledge to divide an industrial process into multiple blocks and then identify an accurate Bayesian Network. The proposed adaptive online alarm threshold optimization algorithm is based on Bayesian Network training and block segmentation.

2.1. Bayesian Network Training

₁₃₀ An essential first step in analyzing alarm information is constructing an alarm propagation network. Bayesian Networks that combine graph models with probability representation are ideally suited for building alarm networks. There are two primary approaches to creating Bayesian Networks: (1) those that are knowledge-driven and (2) those that are data-driven. In recent years, several ₁₃₅ approaches to building data-driven Bayesian Networks have been developed due to easy access to high-quality data from data acquisition systems. Among the data-driven approaches, the Score and Structure (SS) search approach [28] is widely believed to perform better than other methods.

A Bayesian Network is shown in Figure 1, variables $\{x_1, x_2\}$ and $\{x_1, x_3\}$ ₁₄₀ are connected by d_{12} and d_{13}, respectively. In this structure, x_1 is defined as the parent variable, x_2 and x_3 are defined as the child variables. The measurements
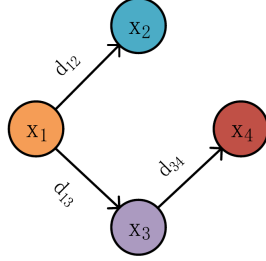
6

Figure 1: The Structrue of the Bayesian Nerwork

from these variables are stored in a data matrix $X = [x_1 \ x_2 \ ... \ x_n]$, $X \in R^{m \times n}$, where n and m represent the number of variables and samples, all parent nodes of x_i are denoted by x_{i_p}, and $x_{i_p}^l$ represents the corresponding sample at the time l. The network of all connected edges is compactly represented using an adjacent matrix as Equation 1.

$$
D = \begin{bmatrix} d_{11} & d_{12} & ... & d_{1n} \\ d_{21} & d_{22} & ... & d_{2n} \\ ... & ... & d_{ij} & ... \\ d_{n1} & d_{n2} & ... & d_{nn} \end{bmatrix} \in R^{n \times n} \tag{1}
$$

where the value of $d_{ij} = 1$ if there is a direct connection $x_i \to x_j$; otherwise $d_{ij} = 0$. The strength of each connection d_{ij} is denoted by θ_{ij}, where $\theta_{ij} \in R^+$ is calculated using functions that measure the corresponding correlation between relevant variables. Some common approaches to find these correlations and score each network are BIC [29], BDE [30], TE [27], etc. Equation 2 represents the strength of all the connections in the network,

$$
\Theta = \begin{bmatrix} \theta_{11} & \theta_{12} & ... & \theta_{1n} \\ \theta_{21} & \theta_{22} & ... & \theta_{2n} \\ ... & ... & \theta_{ij} & ... \\ \theta_{n1} & \theta_{n2} & ... & \theta_{nn} \end{bmatrix} \in R^{n \times n^+} \tag{2}
$$

7

A network can be represented using a graph G, where $G = \langle X, D, \Theta \rangle$ represents one Bayesian Network. Different networks can then be ranked using a score. The score of any structure, where $G_{all} = \{G_1\ G_2\ ...G_T\}$ denotes the set of all possible networks, can be calculated using BIC, BDE, TE, etc. The Score and Search (SS) method defines the best network structure as the structure with the highest score. In other words, the best structure $G_{\max}$ is obtained using Equation 3,

$$G_{\max} = \arg \max_{G_s \in G^{all}} score\,(G_s) \tag{3}$$

Where G_s represents the score for a random network structure, scores obtained using BIC capture the information flow within the structure very well, and the optimal structure obtained by BIC is often relatively straightforward. Compared to the BIC criterion, TE emphasizes information flow within each connection and captures better nonlinear relationships. The BIC scoring criterion is defined as Equation 4.

$$BIC\,(G_s) = \sum_{i=1}^{n} \sum_{j=1}^{q_i} \sum_{k=1}^{r_i} \mathrm{P}_{ijk} \log \left(\frac{\mathrm{P}_{ijk}}{\mathrm{P}_{ij}} \right) - \frac{1}{2} \log\,(m) \sum_{i=1}^{n} (r_i - 1)q_i \tag{4}$$

Where $BIC\,(G_s)$ represents the score for structure G_s, $q_i \in R^+$ and $r_i \in R^+$ represent the number of parent variables and the directed edges of each child variable x_i, respectively, and n represents the number of variables, P_{ijk} is the probability of x_i being in the kth state and x_{p_i} being in the jth state. Therefore $\mathrm{P}_{ij} = \sum_{k=1}^{r_i} \mathrm{P}_{ijk}$ represents the sum of the probability of all different states k of the edge d_{ij}.

The score based on the TE criterion is given as Equation 5.

$$TE\,(G_s) = \sum_{i=1}^{n} T_{x_{i_p} \to x_i} - \lambda \log\,(q_i\,(r_i - 1)) \tag{5}$$

Where $q_i \in R^+$ and $r_i \in R^+$ have the same meaning as above, and λ is a scalar parameter used to penalize the structure complexity. $T_{x_{i_p} \to x_i}$ represents

the transfer entropy value of $x_{i_p} \rightarrow x_i$. The value of TE is calculated as Equation 6.

$$T_{x_{i_p} \rightarrow x} = \sum_{x_i^{t+1}, x_i^t, x_{i_p}^t} p\left(x_i^{t+1}, x_i^t, x_{i_p}^t\right) \log_2 \frac{p\left(x_i^{t+1} \left| x_i^t, x_{i_p}^t \right.\right)}{p\left(x_i^{t+1} \left| x_{i_p}^t \right.\right)} \tag{6}$$

The score based on BDE focuses on the prior probability between variables according to the sampled data X. The resulting structure established by BDE maximizes the posterior probability of all variables. The BDE function is shown as Equation 7.

$$BDE\left(G_s\right) = \sum_{i=1}^{n} \left[\sum_{j=1}^{q_i} \left[\log \frac{\Gamma\left(\alpha_{ij}\right)}{\Gamma\left(\alpha_{ij} + m_{ij}\right)} + \sum_{k=1}^{r_i} \log \frac{\Gamma\left(\alpha_{ijk} + m_{ijk}\right)}{\Gamma\left(\alpha_{ijk}\right)} \right] \right] + \log\left(d_{G_s}\right) \tag{7}$$

Where d_{G_s} represents the number of directed edges in the structure G_s. Γ denotes the standard Gamma function, and $\alpha_{ij} = \sum_{k=1}^{r_i} \alpha_{ijk}$ represents the prior probability between variables. BIC, BDE, and TE scores are widely used to build an optimal structure for Bayesian Networks.

2.2. Multivariate Alarm Threshold Optimization

Improper alarm thresholds can lead to high false and missed alarm rates which can cause either alarm flooding or failure by operators to recognize these alarms in time. Therefore, it is crucial to choose alarm thresholds optimally.

The alarm data are typically binary. Using T_i^t as the threshold of variable x_i at the sampling time t, the process data X and the corresponding alarm data matrix $A = [a_1 \ a_2 \ ... a_n] \in R^{m \times n}$ can be calculated as Equation 8.

$$a_i^t = \begin{cases} 1, & if \quad x_i^t > T_i^t \\ 0, & if \quad x_i^t < T_i^t \end{cases} \tag{8}$$

Where a_i^t represents the alarm data of the ith variable at the sampling moment t.

Traditional multivariate alarm threshold optimization methods can be divided into two types: (1) the first type is based on false and missed alarm rates, and (2) the second type is based on the correlation of alarm sequence and process data. The first type aims to find the right trade-off between false and missed alarm rates by appropriately adjusting the alarm threshold value. The traditional single variable optimization objective function is as Equation 9.

$$J = m_{x_i} + f_{x_i} \tag{9}$$

Where m_{x_i} and f_{x_i} represent the false and missed alarm rates of the x_i at the current threshold, respectively, the corresponding multivariate optimization objective function is given as Equation 10.

$$J = w_1(m_{x_i} + m_{y_i}) + w_2(f_{x_i} + f_{y_i}) \tag{10}$$

Where w_1 and w_2 are appropriate weights for the false and missed alarm rates in the multivariate threshold optimization, but Equation 10 does not evaluate the correlation between the alarm and process data and often cannot accurately balance the relationship between false and missed alarm rates.

The second approach for alarm threshold optimization utilizes the correlation between alarm and process data. If the correlation between alarm and process data is strong, it implies that the alarm threshold is designed correctly, and the alarm data generated by the corresponding threshold can indicate the process conditions. Equation 11 is the corresponding threshold optimization objective function.

$$J = |r_{x_i,y_i} - r_{x_i^a,y_i^a}| \tag{11}$$

Which r_{x_i,y_i} represents the correlation coefficient between the variables x_i and y_i under normal operating conditions, and $r_{x_i^a,y_i^a}$ represents the correlation between the corresponding alarm data of variables x_i and y_i. Both r_{x_i,y_i} and $r_{x_i^a,y_i^a}$ are calculated by process data X and alarm data A according to

10

the corresponding threshold of each variable, and the thresholds are the optimization variables in Equation 11. By maximizing the correlation between the alarm and process data, optimal thresholds can generate alarm data to show the process conditions.

2.3. Modular Decomposition of Process Networks

Typical industrial processes have several variables, and the optimal training of the corresponding Bayesian Network is known to be an NP-hard problem [31]. Moreover, training large networks requires a significant amount of data that are not usually available. An effective way to decrease the complexity of the process is to use a module segmentation algorithm that can reduce the size of the network and hence the amount of data required. This approach also has the added benefit of simplified calculations and improved accuracy of the resulting Bayesian Network. This paper uses the multi-module segmentation technique to reduce the number of variables in each sub-module. The modular decomposition in industrial processes can be completed using the following four steps:

(1) The process is roughly divided into submodules according to process units such as reactors and condensers;

(2) Add a variable between the submodules from (1). Such variables are denoted module-associated variables. In the previous sub-module, module-associated variables cannot have a child node. In the latter sub-module, module-associated variables cannot have a parent node. Based on process knowledge such as chemical process energy flow or control loop, adding the variables between necessary devices to the appropriate sub-modules obtained in the first step;

(3) Complete the search for the Bayesian structure of the respective sub-module;

(4) Merge the submodules using the module-associated variables to obtain a full model/description of the whole system.

3. Algorithm Principle

The state-of-the-art approaches for alarm threshold optimization rely on historical data. However, these approaches cannot guarantee that a given a priori threshold is suitable as the process dynamics change. Therefore, we propose an algorithm to adaptively adjust the alarm threshold at any given sample time using an estimate of the alarming probability at the following sample time. The accuracy of our alarming probability estimates depends on the Bayesian Network used. The scoring metrics for Bayesian Networks identified above focus on the similarity (or correlation) between alarm data rather than the causal relationships between variables, negatively impacting the alarm propagation network's accuracy. To improve the accuracy of the alarm propagation network, in this section, we introduce a concept called Active Transfer Entropy (ATE) and then describe the construction of a simplified multilayers Bayesian Network using active transfer entropy. Once an alarm propagation network is identified, the relevant alarm probabilities will be obtained, which are then used to design adaptive alarm thresholds.

3.1. Simplified Multilayers Bayesian Network based on Active Transfer Entropy

3.1.1. Active Transfer Entropy

Identifying real causal relationships between process variables is essential to building a reliable alarm propagation network. However, commonly used approaches for network analysis are prone to "false causality'' where the correlation between variables is confused with causality. Methods such as TE focus on the similarity between data; therefore, there is a certain probability that they will identify false causal variables. Unlike the traditional TE methods that are often affected by false causality, ATE determines causal relationships with better accuracy. The root cause of false causality is that multiple variables are simultaneously affected by one or more variables, and these affected variables produce similar data characteristics. Hence, finding common cause variables is a key step in eliminating false causality.

12

Let us consider a network with the following four variables $\{x_i, x_j, x_y, x_o\}$. Assume that there are strong correlations between $x_i \to x_o$ and $x_i \to x_j$, as shown in Figure 2.
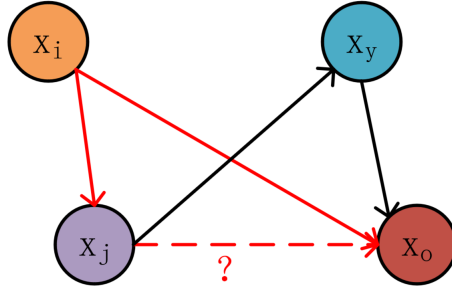

Figure 2: The structure of four variables

As a result, the data correlation between x_j and x_o will be strong. x_i is defined as the common cause of $x_j \to x_o$. We find the common cause variables using the traditional transfer entropy calculations. The calculation of the traditional transfer entropy is performed as Equation 6, and the following criterion judges the existence of the relationship between the variables.

$$T_{(x_{i_p} \to x_i)^{nor}} = T_{x_{i_p} \to x_i} - \sum_{t=1}^{tall} \frac{T_{(x_{i_p} \to x_i)_t^r}}{tall} \tag{12}$$

Where $T_{(x_{i_p} \to x_i)^{nor}}$ represents the transfer entropy of $x_{i_p} \to x_i$ after normalizing, $T_{(x_{i_p} \to x_i)_t^r}$ represents the transfer entropy from the tth random shuffle of x_{i_p} to x_i, and $tall$ represents the times of randomizing the sampling data of variables. The common cause variables of the $x_j \to x_o$ are denoted by x_{j_p}. We use the positivity of the corresponding transfer entropy to determine if there exists a common cause variable.

$$T_{(x_{j_p} \to x_j)^{nor}} > 0 \tag{13}$$

If a variable is not correlated with x_j, then the corresponding transfer entropy in Equation 12 will be a non-positive value. Therefore, if $T_{(x_{j_p} \to x_j)^{nor}} > 0$, x_{j_p} is defined as the common cause variable of $x_j \to x_o$.

As shown in Figure 2, x_i is the parent variable of x_j, and x_y is the intermediate node of x_j and x_o. When calculating the transfer entropy of $x_j \to x_o$, x_i is regarded as a common cause variation. In the same way, if calculating the transfer entropy of $x_y \to x_o$, x_j is the parent node of x_y and is regarded as a common cause variable. Considering that both x_y and x_o have eliminated the information from x_j, if path $x_y \to x_o$ has a small transfer entropy value, it means that x_y and x_o are both influenced by x_j, and these two variables have no causal relationship.

After obtaining the common cause variable x_{i_c} from binary alarm data, the discretized ATE is calculated as Equation 14.

$$
\begin{aligned}
ATE_{x_{i_p} \to x_i} = &\sum_{x_i^{t+1}, x_i^t, x_{i_c}^t, x_{i_p}^t} p\left(x_i^{t+1}, x_i^t, x_{i_c}^t, x_{i_p}^t\right) \log_2 \frac{p\left(x_i^{t+1} \middle| x_i^t, x_{i_c}^t, x_{i_p}^t\right)}{p\left(x_i^{t+1} \middle| x_i^t, x_{i_c}^t\right)} \\
&- \sum_{x_{i_p}^{t+1}, x_p^t, x_{i_c}^t, x_i^t} p\left(x_{i_p}^{t+1}, x_p^t, x_{i_c}^t, x_i^t\right) \log_2 \frac{p\left(x_{i_p}^{t+1} \middle| x_p^t, x_{i_c}^t, x_i^t\right)}{p\left(x_{i_p}^{t+1} \middle| x_p^t, x_{i_c}^t\right)}
\end{aligned}
\tag{14}
$$

Unlike the traditional transfer entropy scoring criterion, the active transfer entropy provides a better estimate of causal relations. In the next section, we will use ATE to identify a more accurate alarm propagation network.

3.1.2. Network structure search

Once the value of the active transfer entropy between the process variables is calculated, we use a greedy search algorithm to search for the optimal Bayesian Network structure. Each network structure is scored by Equation 15.

$$Score_{\text{ATE}}\left(G_{greedy}\right) = \sum_{i=1}^{n}\left(\sum_{x_i^{t+1},x_i^t,x_{i_c}^t,x_{i_p}^t} p\left(x_i^{t+1},x_i^t,x_{i_c}^t,x_{i_p}^t\right)\log_2\frac{p\left(x_i^{t+1}\middle|x_i^t,x_{i_c}^t,x_{i_p}^t\right)}{p\left(x_i^{t+1}\middle|x_i^t,x_{i_c}^t\right)}\right.$$

$$\left. - \sum_{x_{i_p}^{t+1},x_p^t,x_{i_c}^t,x_i^t} p\left(x_{i_p}^{t+1},x_p^t,x_{i_c}^t,x_i^t\right)\log_2\frac{p\left(x_{i_p}^{t+1}\middle|x_p^t,x_{i_c}^t,x_i^t\right)}{p\left(x_{i_p}^{t+1}\middle|x_p^t,x_{i_c}^t\right)}\right)$$

$$- \lambda_1\log\left(n\right)$$

$$= \sum_{i=1}^{n}\left(ATE_i\right) - \lambda_1\log\left(n\right)$$

$$(15)$$

Where n is the number of directed edges obtained by greedy search, λ_1 is the penalty coefficient used to limit the structural complexity. The final optimal Bayesian Network structure is determined as Equation 16.

$$G_{\max} = \arg\max_{G_{greedy}\in G^{all}} Score_{\text{ATE}}\left(G_{greedy}\right) \qquad (16)$$

3.1.3. Simplified Multilayer Bayesian Network (SMBN)

The alarm propagation structure obtained by ATE can accurately express the relationship between variables. However, the alarm data are binary, and they alone are not suitable for predicting future alarms. To account for the lack of sufficient information in binary alarm data, multi-layer Bayesian networks with temporal information, such as dynamic Bayesian networks, have been recently studied by Perrin [32]. Figure 3 and Figure 4 show two different kinds of dynamic Bayesian networks. Each variable in Figure 3 is connected to each node of the previous layer. This multi-layer Bayesian Network requires large volumes of data for training. On the other hand, the structure in Figure 4 is simple, but it is difficult to provide accurate information for analyzing alarm propagation as only a few vital nodes are connected.

We combine the simple form in Figure 4 with the ATE scores defined earlier to ensure that structure is manageable and performs better. We propose a
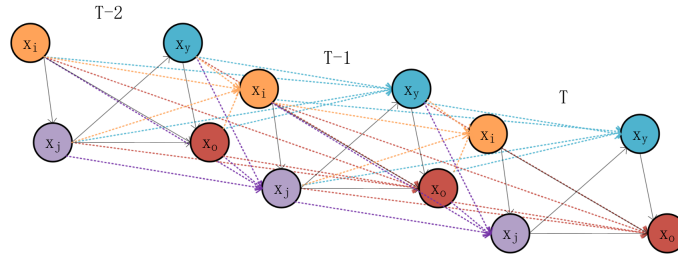
15

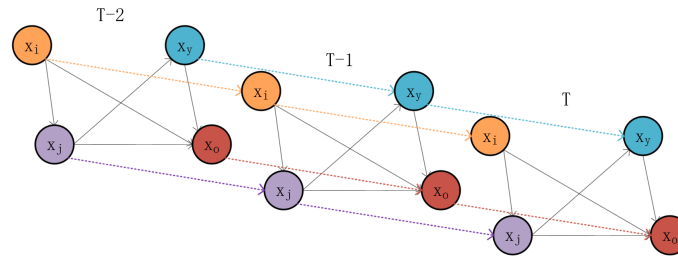Figure 3: The structure of a fully connected dynamic Bayesian network

Figure 4: The structure of traditional dynamic Bayesian network

three-layer alarm network structure based on ATE called SMBN-ATE, shown in Figure 5.
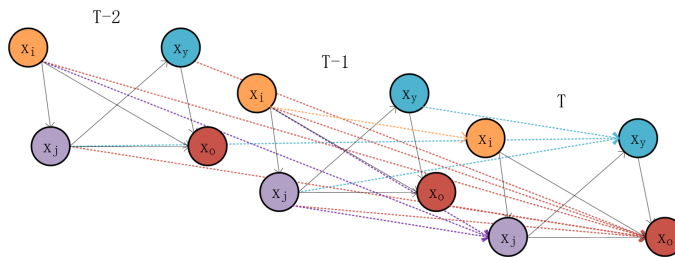

Figure 5: The structure of ATE-based simplified multilayers Bayesian network

For the relationships between variables as given in Figure 2, the corresponding SMBN-ATE will be the network shown in Figure 5. Unlike typical Markov processes where the variables at the current time instant only depend on the variable at the previous instant, the above three layers of SMBN-ATE allows

for connections between the variables and their parent nodes in the first two layers. This three-layer alarm propagation structure can reduce the complexity and improve the stability of Bayesian network parameter learning by causal inference and provide better alarm data information for alarm prediction. In the simulation section, we analyze the SMBN-ATE structure and illustrate the suitability of this approach in adaptive online optimization of alarm thresholds.

3.2. Adaptive online optimization of alarm threshold

The adaptive online optimization method is designed to adjust the threshold to adapt to the upcoming alarms using the estimated alarm probability. Therefore, accurate prediction of alarms is essential for our approach. Bayesian Network parameter training is carried out according to Section 3.1.2. Each variable's prior probability of alarms is calculated by parameter training in the Bayesian network. In the actual process, the alarm probability value P_v^t is calculated by the alarm data of all parent variables of v, where v represents the variable to be optimized, t represents the sample time, and the alarm data is obtained by Equation 8. The inference of P_v^t is done with the Bayesian inference toolbox in this paper, and other types of classifiers can also perform probability calculations.

Since P_v^t changes at each sample instant, we use Equation 17 to determine whether the threshold of each variable needs to be adjusted.

$$P_v^t > OP_v \tag{17}$$

Where OP_v is a user-defined probability threshold, the OP_v is chosen to ensure that the alarms whose alarm probability is greater than OP_v contain 80% of all alarms of the variable. This choice guarantees that the threshold is optimized before critical alarms occur, and the setting of OP_v is calculated by the analysis of historical data. In practical applications, if a variable cannot be set OP_v to ensure that 80% of alarms are detected, it is important to prove that the variable has significant fluctuations and is not applicable to adaptive threshold optimization.

The adaptive threshold optimization method works with Equation 18 as the objective function based on the alarming probability P_v^{t+1} in the next sample, where the optimization algorithm can use the greedy algorithm, etc, and the calculation of alarm probability can be calculated by the Bayesian inference or other superior classifiers. In the experiments of this paper, all parent variables of v were defined as input, and the inference of P_v^{t+1} is calculated by the Bayesian inference toolbox.

$$J = \min \left| \left(\frac{1 - e^{-L_v P_v^{t+1}}}{1 + e^{-L_v P_v^{t+1}}} \right) m_v + \left(\frac{2e^{-L_v P_v^{t+1}}}{1 + e^{-L_v P_v^{t+1}}} \right) f_v \right| \tag{18}$$

Where L_v is a measure of the importance of the variable v, and m_v and f_v represent the missed and false alarm rates of the variable v, respectively. The threshold optimization of each variable is only performed while the alarm is between the double-high alarm and the double-low alarm set by operators. Once the double-high alarm is exceeded, or the double-low alarm is exceeded, appropriate physical measures must be taken to prevent catastrophic events. A large value is chosen for the most critical variables, a medium value is chosen for normal variables, and a low value is chosen for less critical variables.

The adaptive online alarm threshold optimization strategy proposed in this paper allows for tight alarm thresholds when the alarming probability of the variable is high. Similarly, when the alarming probability of a variable is low, a larger threshold is used to reduce the false alarm rate. The overall algorithm is summarized in Figure 6, and a detailed description of each of these steps is shown below.

(1) Dividing necessary equipment into sub-modules based on industrial process knowledge;

(2) Defining the module-associated variables between sub-modules obtained in the first step as described in Section 2.3;

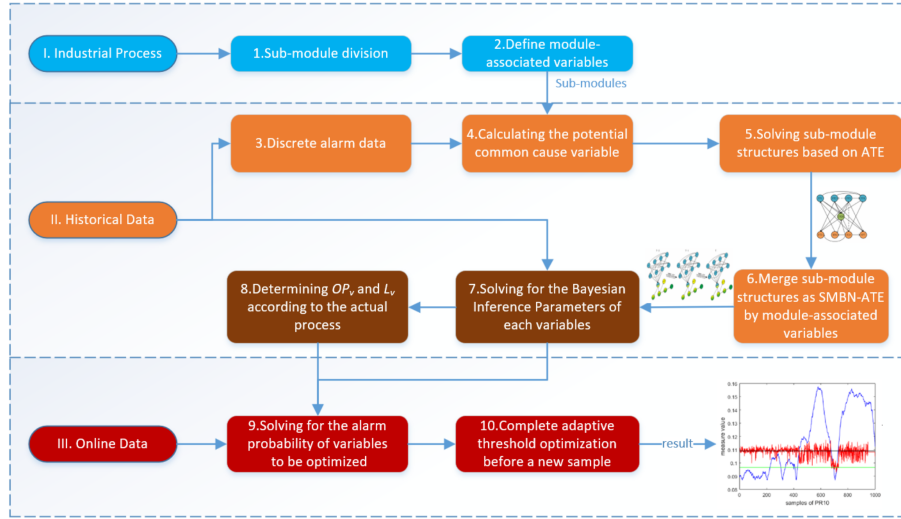(3) Converting historical sampling data to binary alarm data according to Equation 8;

18

Figure 6: The flow chart of the adaptive online alarm threshold optimization method based on SMBN-ATE

(4) Solving for the potential common cause variables in each submodule according to Equation 12 and 13;

(5) Constructing the structure of each submodule is based on Equation 15 and Equation 16, each edge in the structure represents a causal rather than a correlative relationship for alarm propagation;

(6) Reconstructing multiple sub-modules as SMBN-ATE structure through module-associated variables to obtain the final structure for threshold optimization, as shown in Figure 5;

(7) The training of the parameters required for Bayesian inference is completed by historical data to obtain the conditional probabilities of alarms between variables and their parent nodes;

(8) Combining process knowledge and historical data to complete the OP_v and L_v settings ensures that more than 80% of historical alarms can be further optimized;

(9) Selecting variables to be optimized at the next moment base on the online data at each moment according to Equation 17;

19

(10) Using Equation 18 as the objective function, the alarm threshold of the variable to be optimized at the next moment is solved, and finally, adaptive threshold optimization is achieved.

4. Experiments

This section presents two experiments to demonstrate the previously described method. In the first experiment, we evaluate three Bayesian network structure scoring algorithms based on micro-seismic data from an actual mining process. In the second experiment, we use the Tennessee Eastman Process (TEP) data to demonstrate the adaptive threshold optimization approach proposed in this paper in detail and further prove the effectiveness and superiority of the proposed method.

4.1. Coal mine process

In the Coal mining process, rock bursts occasionally occur and result in worker fatalities. There is no established method for predicting rock bursts, which makes coal mining an exceedingly risky operation. It is vital to recognize the anomalous data and determine the rock burst position at the earliest possible stage of rock burst occurrence by solving the propagation path of the anomalous micro-seismic energy and comparing it with the actual monitor's position. This section compares the performance of BIC, BDE, and ATE structural search scoring methods using anomalous micro-seismic data collected in a coal mine at 00:15 on June 16, 2016.

As illustrated in Figure 7, the dataset contains monitoring information from nine micro-seismic monitors for four hours, totaling 10240 samples. Since numerous micro-seismic monitors are positioned throughout the mine, monitors 1, 4, 6, 7, 8, and 9 cannot detect attenuated micro-seismic signals. In this experiment, the propagation path of the micro-seismic signal is solved using a total of three monitors capable of receiving micro-seismic signals: monitors 2, 3, and 5. In this research, the same time window is employed in keeping with

20

the size of the analysis sample width of 400 for micro-seismic analysis in the actual coal mine. The analysis is calculated from the 7300th data to the 7700th data, as shown in Figure 7. The ground truth of this anomalous event is that the source of the rock burst is closest to monitor 3, followed by monitor 5, and finally propagates to monitor 2.
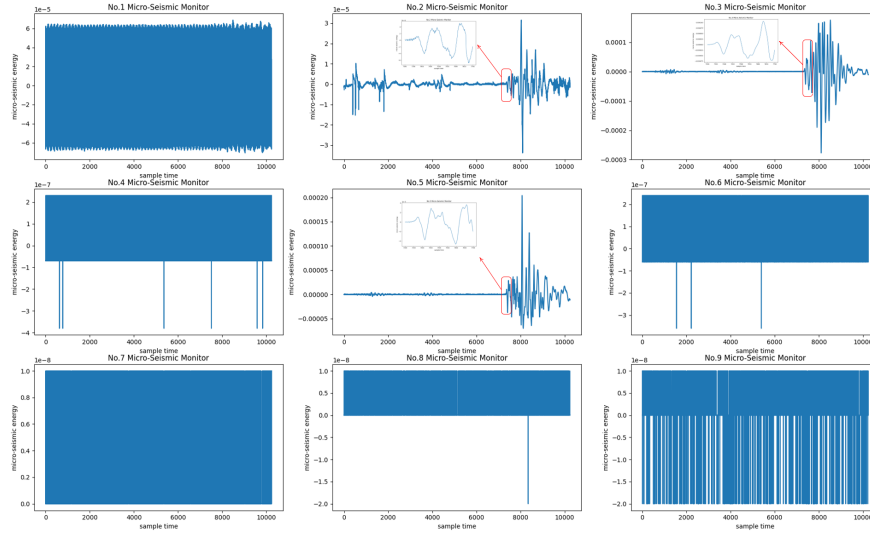

Figure 7: The data of nine micro-seismic monitors

The results of the propagation structure search by BIC, BDE, and ATE are illustrated in Figure 8 (a), Figure 8 (b), and Figure 8 (c), respectively. BIC, BDE, and ATE accurately calculated that monitor 3 was the first device to monitor the source signal, and both accurately obtained the directed edge from monitor 3 to monitor 2. However, as BIC and BDE consider more the correlation between data than the causality, they both achieve the opposite conclusion from monitor 2 to monitor 5, and the BIC approach also misses the directed edge from monitor 3 to monitor 5. In contrast, the ATE-based structure search method concentrates on the calculation of causality between data and obtains a total of three proper propagation relations from monitor 3 to monitor 2, monitor 3 to 5, and monitor 5 to monitor 2.

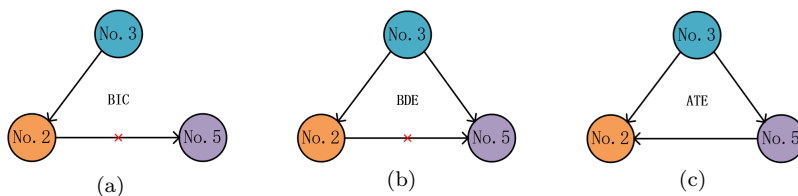This experiment based on actual data demonstrates that in practical en-

21

Figure 8: Results of propagation structure solution based on BIC, BDE and ATE scoring method: (a) BIC; (b) BDE; (c) ATE

gineering applications, compared with the traditional BIC and BDE scoring criteria, the ATE score-based propagation structure learning method can reduce the interference of false-causal relationships between data and thus obtain a more objective and complete relationship between monitoring data, which is of practical significance. A more comprehensive SMBN structure search and threshold optimization will be described in detail in Section 4.2.

4.2. Tennessee Eastman process

The TEP [33, 34, 35] is a benchmark process provided by the Tennessee Eastman Company. Due to the comprehensiveness and complexity of data, it is often used as a benchmark in fault detection and alarm analysis research. The structure of TEP is shown in Figure 9. The process is controlled by 12 control variables XMV (1-12), where XMV (1-11) are 11 commonly used control variables. The overall process is monitored by 41 measured variables XMEAS (1-41), of which XMEAS (1-22) are 22 commonly used measurement variables, as shown in Table 1. Given that the SMBN-ATE-based adaptive online optimization method applies to complex chemical systems, we demonstrate the effectiveness of the proposed method using the TEP process. Three traditional Bayesian structure search methods, BIC, BDE, and MBTE [27], are used for simulation. The traditional univariate threshold setting and False Alarm Probability and Missing Alarm Probability (FAP-MAP) threshold optimization method are used for comparison. In this paper, we use the Fault 1 dataset from TEP for the experiment. This dataset has 1000 samples with 3 minutes between

22

each sample, where the first 400 samples are normal and the fault is brought in
at the 401st moment, so the last 600 samples are abnormal data. In the first 400
samples, if the sampled value is greater than the alarm threshold, it is defined
as a false alarm. And in the last 600 samples, if the sampled value is less than
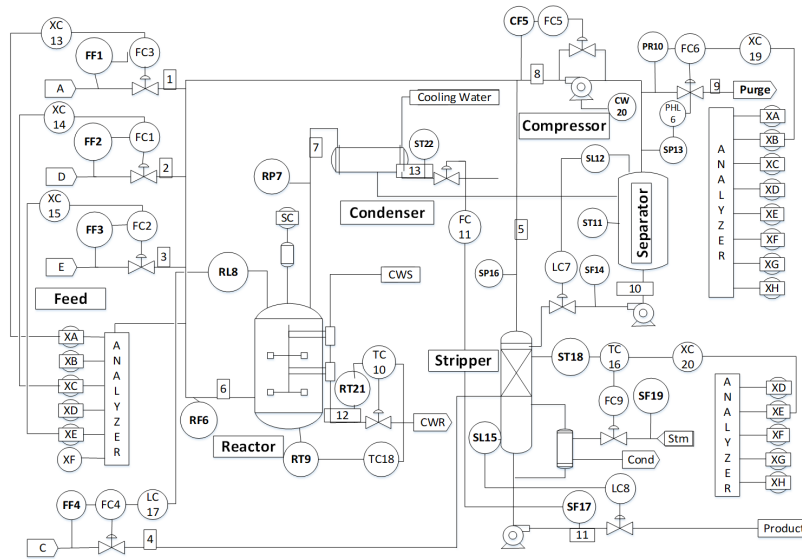the alarm threshold, it is classified as a missing alarm.

Figure 9: The description of the TE process [34]

4.2.1. Modular Decomposition

In the data of IDV1, the alarming probability of each variable under normal
and abnormal working conditions is shown in Figure 10. The variables are
further pruned before performing a structural search according to the calculation
of alarm probability, and the variables are considered unrelated to the IDV1 fault
and removed once the alarming probability do not change significantly.

To reduce the number of required data and improve computational efficiency,
we divide the TEP process into three sub-modules according to the constraints
of process knowledge. As shown in Table 2, CW20 belongs to both Sub-module1
and Sub-module2, and is defined as a module-associated variable of Sub-module1
and Sub-module2; ST11, SP13, and ST22 belong to both Sub-module2 and

23

Table 1: The description of 22 measured variables in the TE process [27]

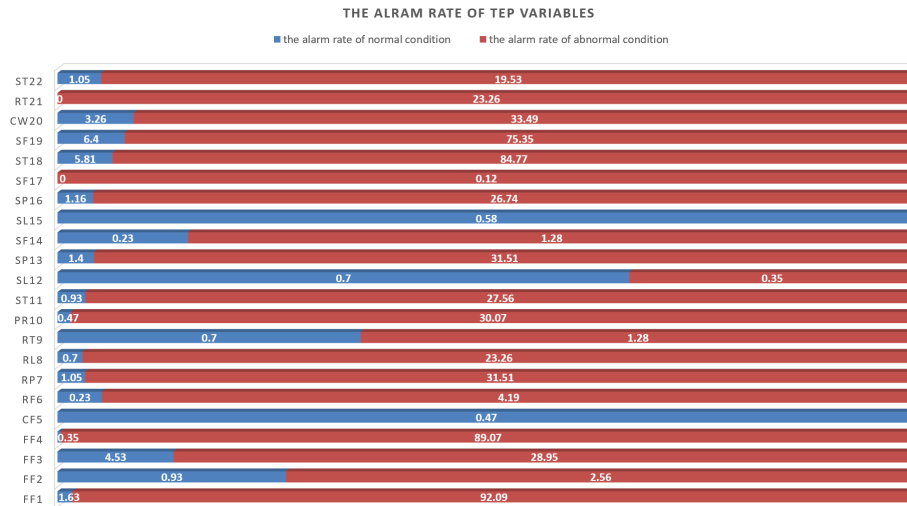| Variable number	Variable symbol	Type	Unit
FF1	XMEAS(1)	A feed (stream 1)	
FF2	XMEAS(2)	D feed (stream 2)	Feed
FF3	XMEAS(3)	E feed (stream 3)	
FF4	XMEAS(4)	Total feed (stream 4)	
CF5	XMEAS(5)	Recycle flow (stream 8)	Compressor
RF6	XMEAS(6)	Reactor feed rate (stream 6)	
RP7	XMEAS(7)	Reactor pressure	Reactor
RL8	XMEAS(8)	Reactor Level	
RT9	XMEAS(9)	Reactor temperature	
PR10	XMEAS(10)	Purge rate (Stream 9)	Purge
ST11	XMEAS(11)	Product set temp	
SL12	XMEAS(12)	Product set level	Separator
SP13	XMEAS(13)	Product set pressure	
SF14	XMEAS(14)	Product set underflow (stream 10)	
SL15	XMEAS(15)	Stripper level	
SP16	XMEAS(16)	Stripper pressure	
SF17	XMEAS(17)	Stripper underflow (stream 11)	Stripper
ST18	XMEAS(18)	Stripper temperature	
SF19	XMEAS(19)	Stripper steam flow	
CW20	XMEAS(20)	Compressor work	Compressor
RT21	XMEAS(21)	Reactor cooling water outlet temp	Reactor
ST22	XMEAS(22)	Separator cooling water outlet temp	Separator

THE ALRAM RATE OF TEP VARIABLES

■ the alarm rate of normal condition ■ the alarm rate of abnormal condition

Variable	normal condition	abnormal condition
ST22	1.05	19.53
RT21	0	23.26
CW20	3.26	33.49
SF19	6.4	75.35
ST18	5.81	84.77
SF17	0	0.12
SP16	1.16	26.74
SL15	0.58	0
SF14	0.23	1.28
SP13	1.4	31.51
SL12	0.7	0.35
ST11	0.93	27.56
PR10	0.47	30.07
RT9	0.7	1.28
RL8	0.7	23.26
RP7	1.05	31.51
RF6	0.23	4.19
CF5	0.47	0
FF4	0.35	89.07
FF3	4.53	28.95
FF2	0.93	2.56
FF1	1.63	92.09

Figure 10: The alarm rate under normal condition and IDV(1)

Sub-module3, these variables are defined as module-associated variables of Sub-module2 and Sub-module3. When the sub-module structure is established, the common variables will be used to reconstruct the overall process structure.

Table 2: The optimal sub-modules of TE process

sub-modules	units	variables
Sub-module1	Feed, reactor, condenser, compressor, venting	FF1,FF2,FF3,FF4,RF6, RP7,RL8,RT21,CW20
Sub-module2	Condenser, compressor, Venting, separator	CW20,PR10,ST11, SP13,ST22
Sub-module3	Separator (part), stripper	ST11,SP13,ST22, SP16,ST18,SF19

4.2.2. SMBN-ATE calculation

Determining the common cause variables is a crucial step for ATE calculation. Since these calculations are similar for each sub-module, we focus on

Sub-module1 as an example. The relationship of each variable in Sub-module1 is calculated according to Equation 12, and the results are shown in Figure 11.
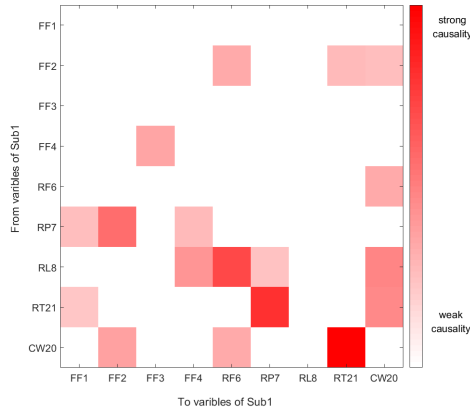

Figure 11: The TE value of variables in Sub-module1

In Figure 11, the vertical axis represents the parent node variable, and the horizontal axis represents the child node variable. Since RP7 and CW20 have strong transfer relationships to FF2, RP7 and CW20 are defined as common cause variables of FF2. Summarizing the information in Figure 8, the edges from potential common cause variable to each variable in Sub-module1 are given in Table 3.

Taking common cause variables into the calculation of ATE, the value of the active transfer entropy between variables is calculated by Equation 14, and is shown in Figure 12.

Because variables in the graph have different degrees of transfer relationship, we use the ATE values in Figure 12 in the structure search algorithm to obtain a single-layer Bayesian Network structure to get a more accurate network structure. Figure 13, Figure 14, Figure 15, and Figure 16 show the network structure using BIC, BDE, and MBTE methods in combination with the ATE method proposed in this paper.

In Figure 13, Figure 14, Figure 15, and Figure 16, the red lines represent the data-driven Bayesian Network structure missing some important process

26

Table 3: The edges from potential common cause variable to each variable in Sub-module1

Variable	The edges from potential common cause variable
FF1	RP7 → FF1,RT21 → FF1
FF2	RP7 → FF2,CW20 → FF2
FF3	FF4 → FF3
FF4	RP7 → FF4,RL8 → FF4
RF6	FF2 → RF6,RL8 → RF6,CW20 → RF6
RP7	RL8 → RP7,RT21 → RP7
RL8	None
RT21	FF2 → RT21,CW20 → RT21
CW20	FF2 → CW20,RF6 → CW20,RL8 → CW20,RT21 → CW20
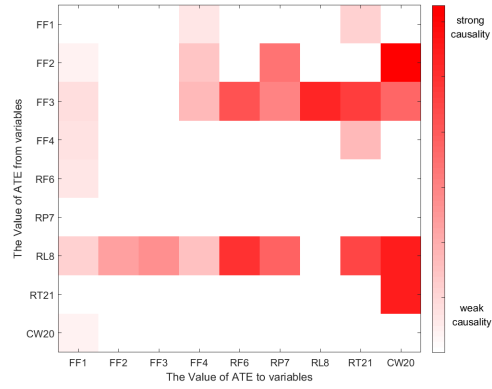
Figure 12: The ATE value of variables in Sub-module1
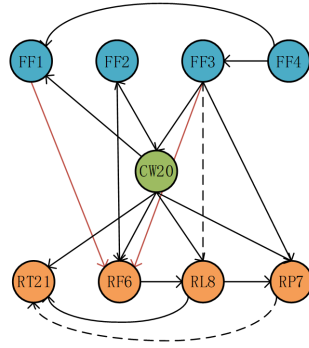
27

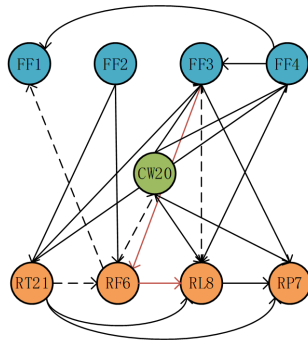Figure 13: The structure of Sub-module1 searched based on the BIC method

Figure 14: The structure of Sub-module1 searched based on the BDE method
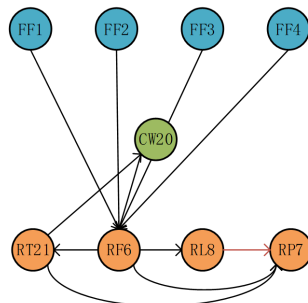

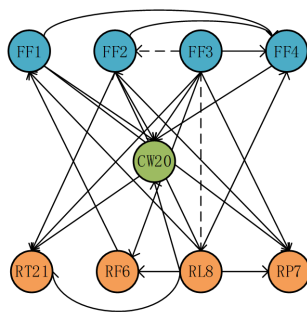Figure 15: The structure of Sub-module1 searched based on the MBTE method

Figure 16: The structure of Sub-module1 searched based on the ATE method

relationships; the black lines represent the relationships in the structure that are consistent with the actual process, and the dashed lines represent the opposite relationships of the actual process. The structures obtained by BIC and BDE have certain important relationships missing. Although the structure of MBTE is better than the BIC and BDE methods, the important relationship between RL8 and RP7 is still missing. However, the ATE method not only constructs an accurate propagation relationship but also solves the problem of false causality. For example, RF6 is the reactor feed rate, and RP7 is the reactor pressure. RF6 is affected by feed rates of FF1, FF2, and FF3, so there is only a similarity between RF6 and RP7 rather than causality. The ATE-based method does not construct the relationship between RF6 and RP7 and constructs the relationship from FF1, FF2, and FF3 to RF6 and Rp7. Different from MBTE, with ATE, we can avoid false causal relationships. The statistics of the results are shown in Table 4, where Y, B, and N represent correct, opposite, and erroneous results, respectively.

This example illustrates that ATE is better able to construct Bayesian networks. The parent node and child nodes of each edge in the reconstructed overall process are shown in Table 5, and the ATE-based single-layer Bayesian Network structure is shown in Figure 17.

After obtaining the single-layer Bayesian Network structure, based on the discussion in Section 3.1.2, we extended the structure into a three-layer SMBN-ATE structure, as shown in Figure 18. In this three-layer structure, variables

29

Table 4: The results of the BDE, BIC, MBTE and ATE structure learning method

Method	Y	B	N	Correct rate
BDE	16	4	2	72.7%
BIC	14	2	2	77.8%
MBTE	10	1	0	90.9%
ATE	22	2	0	91.7%

Table 5: The parent node and child nodes of each edge in the reconstructed structure

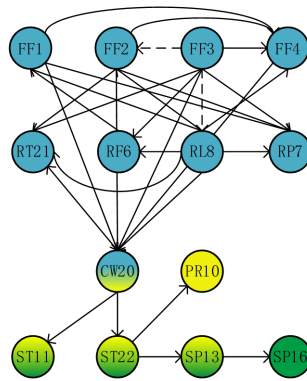| Parent Node	Child Nodes	Parent Node	Child Nodes
FF1	FF4,RP7,CW20	RT21	None
FF2	FF4,RP7,CW20,RT21	PR10	None
FF3	FF2,FF4,RF6,RP7,RL8,CW20,RT21	ST11	None
FF4	CW20	SP13	SP16
RF6	FF1	ST22	PR10,ST11,SP13
RP7	None	SP16	None
RL8	FF1,FF2,FF4,RF6,RP7,CW20,RT21	ST18	None
CW20	RT21,ST11,ST22	SF19	None

Figure 17: The searched structure based on ATE method

Table 6: The optimization parameters of different variables

Variable	FF 1	FF 2	FF 3	FF 4	RF 6	RP 7	RL 8	PR 10	ST 11	SP 13	SP 16	SF 19	CW 20	ST 22
OP_v	0.4	0.2	0.1	0.3	0.2	0.4	0.4	0.2	0.2	0.2	0.4	0.1	0.2	0.4
L_v	2	2	2	2	1	3	3	2	2	3	2	3	1	2

are only connected to the parent nodes of the previous two layers. They are also connected to their nodes of the previous layer. The SMBN-ATE structure will be used to calculate the parameters of the adaptive online alarm threshold optimization method in Section 4.2.3.
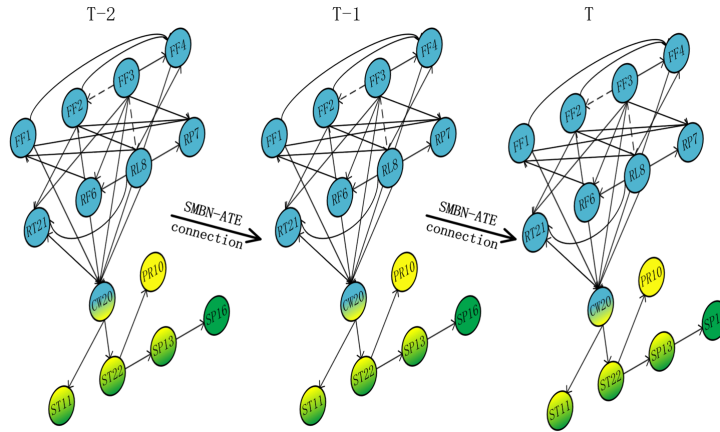

Figure 18: The structure of Simplified Multilayers Bayesian network based on ATE

4.2.3. Adaptive online optimization

According to the three-layer Bayesian Network structure in Figure 18, the relationship between the variables is constructed for the parameter training of the Bayesian network. According to Equation 17 and Equation 18, we first set the OP_v and L_v values of 14 variables, as shown in Table 6.

The setting of the OP_v must ensure the alarm prediction probability can cover 80% of alarms. Based on this condition, the value of OP_v needs to be 0.23.

The smaller the value of OP_v represents the more frequently the variable v is tested for threshold optimization. To ensure that more alarms can be included, OP_v is approximated to 0.2. The level is set according to the importance of variables in the process, the larger the value of L_v represents the more important the variable v is. This paper use three levels of alarms, and the crucial alarms are defined as level-3 alarms. In practical engineering applications, OP_v and L_v are two key parameters that designers need to calculate based on historical data or decide the importance of the variables based on the process design.

According to the objective function in Equation 18, we perform the calculation on a regular computer with an i7 CPU and 16G RAM, it takes 2 minutes to complete the threshold optimization for all variables at each sample, which is less than 3 minutes for a single sample in TEP. In real industry, more powerful computing capabilities will also further make the computational burden no longer a problem. The result of the adaptive online optimization of IDV1 is shown in Figure 19.

The blue line represents the sampled value of each variable, the black line is the traditional univariate threshold, and the green line is the threshold obtained by the FAP-MAP-based multivariate threshold optimization method. It is important to note that there are three kinds of threshold lines in each figure, but in some figures, the green and black lines overlap. The red line is the threshold based on the SMBN-ATE adaptive online optimization method. Through the optimization curves of RL8, ST22, SP16, and FF3 in Figure 19 (a), when the IDV1 fault occurs, the adaptive online alarm threshold optimization method proposed in this paper makes the alarm threshold stricter, which means the threshold value decreases to give more accurate alarms. Similarly, it can be seen from Figure 19 (b) that the red line will still be adaptively adjusted to the optimization curves of FF2, RF6, RP7, PR10, ST11, and ST13 according to different alarm probabilities at each sample. For example, at the 700th sample of PR10, the process is still in the fault state; However, the value of PR10 returns to the normal interval, the PR10 still has a high alarm probability, and the threshold represented by the red line adaptively decreases to provide an

32

(a)

(b)

(c)

33
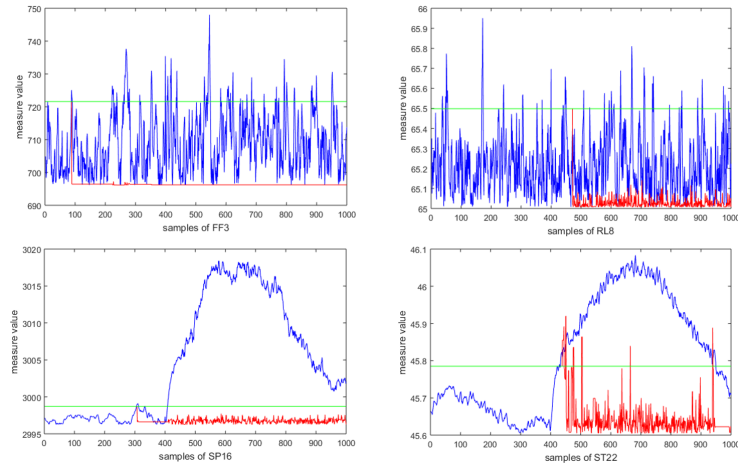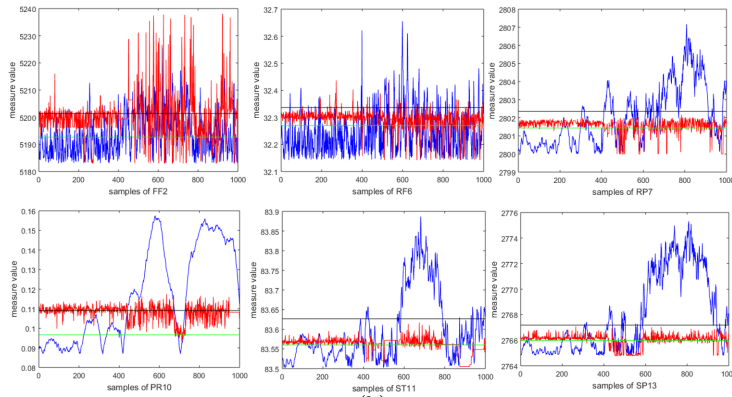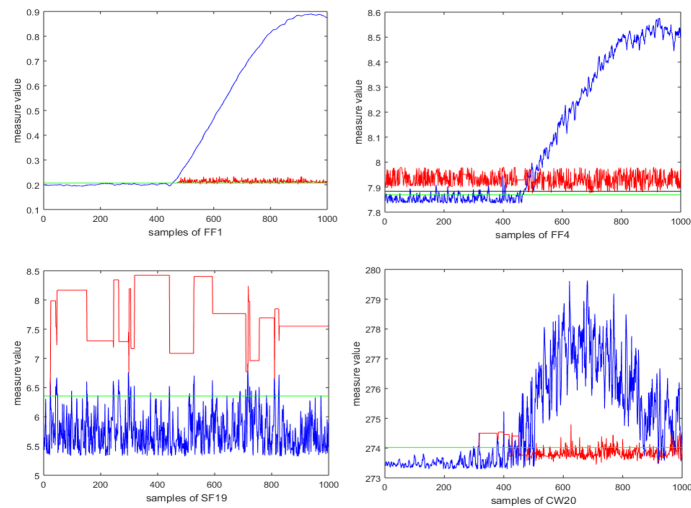
Figure 19: The threshold optimization results are based on a univariate threshold, FAP-MAP method, and SMBN-ATE method. (a) FF3, RL8, SP16, ST22; (b) FF2, RF6, RP7, PR10, ST11, ST13; (c) FF1, FF4, SF19, CW20.

accurate alarm. For the optimization curve of alarm variable SF19 in Figure 19

₅₇₅ (c), noticing that SF19 rarely has an alarm, the threshold adaptively becomes loose to reduce the false alarm rate. Finally, the false and missed alarm rates corresponding to the three methods are shown in Table 7.

Table 7: The false alarm rate and missing alarm rate of univariate threshold, FAP-MAP method, and SMBN-ATE method

Vari-ables	FAR-Uni	FAR-FAP-MAP	FAR-SMBN-ATE	MAR-Uni	MAR-FAP-MAP	MAR-SMBN-ATE	Sum-Uni	Sum-FAP-MAP	Sum-SMBN-ATE
FF1	0.000	0.000	**0.000**	0.090	0.090	**0.090**	0.054	0.054	**0.054**
FF2	0.030	0.258	0.073	0.720	0.358	0.613	0.444	0.318	0.397
FF3	0.080	0.080	0.765	0.892	0.892	**0.005**	0.567	0.567	**0.309**
FF4	0.048	0.155	**0.000**	0.110	0.088	0.155	0.085	0.115	0.093
RF6	0.045	0.173	0.088	0.795	0.598	0.640	0.495	0.428	**0.419**
RP7	0.030	0.163	0.103	0.392	0.213	**0.182**	0.247	0.193	**0.15**
RL8	0.053	0.053	**0.053**	0.933	0.933	**0.160**	0.581	0.581	**0.117**
CW20	0.000	0.353	0.008	0.153	0.073	0.122	0.092	0.185	**0.076**
RT21	0.003	0.303	0.213	0.578	0.287	**0.280**	0.348	0.293	**0.253**
PR10	0.015	0.218	0.160	0.300	0.175	**0.072**	0.186	0.192	**0.107**
ST11	0.000	0.000	**0.000**	0.205	0.205	**0.205**	0.123	0.123	**0.074**
SP13	0.075	0.075	**0.003**	0.950	0.950	0.997	0.600	0.600	**0.599**
ST22	0.033	0.033	**0.018**	0.118	0.118	**0.105**	0.084	0.084	**0.07**
SP16	0.000	0.000	**0.000**	0.135	0.135	**0.065**	0.081	0.081	**0.039**
ST18	0.000	0.000	**0.000**	0.090	0.090	**0.090**	0.054	0.054	**0.054**
SF19	0.030	0.258	0.073	0.720	0.358	0.613	0.444	0.318	0.397
Mean	0.029	0.133	0.106	0.455	0.365	**0.264**	0.285	0.272	**0.197**

In Table 7, Uni, FAP-MAP, and SMBN-ATE represent the default univariate threshold, the multivariate optimization threshold based on the FAP-MAP, and

₅₈₀ the adaptive online optimization method proposed in this paper. FAR, MAR, and Sum represent the false alarm rate, the missed alarm rate, and the alarm information error rate, respectively. The last row in Table 7 shows the average false alarm rate, the average missing alarm rate, and the sum of the average false alarm and the average missing rate for the 16 variables. It can be found

₅₈₅ that the proposed SMBN-ATE method optimizes the average false alarm rate

34

from 13.3% to 10.6% compared with FAP-MAP. At the same time, SMBN-ATE has an excellent performance in the average missing alarm rate, which has significantly improved from 45.5% and 36.5% to 26.4% compared with Uni and FAP-MAP, respectively. The sum of the average false alarm rate and the average missing alarm rate shows that the results of Uni and FAP-MAP are 28.5% and 27.2%, respectively, and the proposed SMBN-ATE method is only 19.7%, which has a significant improvement.

4.2.4. Discussion

With the proposed SMBN-ATE adaptive online optimization approach, a significant improvement of the false and missed alarm rates is completed in TEP. Compared to the traditional threshold optimization methods, where a trade-off between false and missed alarm rates is required, the proposed method independently adjusts the false and missed alarm rates. Our approach depends critically on predicting the alarming probability of the following sampling. Therefore, the missed and false alarm rates can be optimized simultaneously. In Table 7, the column of alarm information error rate (Sum) shows that our proposed achieved results in which alarm performance of more than 80% of the variables has improved. In addition to the excellent performance shown in Table 7, the SMBN-ATE-based adaptive online alarm threshold optimization method also has better applicability in practical industrial applications. The core principle of SMBN-ATE for threshold optimization is based on Bayesian inference, so only threshold optimization for linear faults can be accomplished with a limited amount of data. However, since the alarm propagation structure is constructed based on information entropy, which is suitable for nonlinear data. As a result, the method proposed in this paper can still accomplish the threshold optimization for nonlinear faults in the real industry as long as the historical data is sufficient. We believe that the method proposed in this paper should be further enhanced if simple Bayesian inference is replaced by methods such as graph neural networks. In summary, the SMBN-ATE-based adaptive online alarm threshold optimization method reduces undesirable alarms, prevents

35

alarm flooding, and improves the overall safety of a process.

5. Conclusions

An SMBN-ATE-based adaptive online alarm threshold optimization method is proposed in this paper. It can optimize alarm thresholds before alarms occur, improve the accuracy of alarms, and help operators to obtain and handle alarm information in time to ensure the safety of industrial processes. The SMBN-ATE-based method proposed in this paper includes modular segmentation, constructing a multi-layer alarm propagation network, and adaptive online optimization of alarm thresholds. Compared with traditional alarm threshold optimization methods, our method first distinguishes correlation from causality while searching for optimal network structure. This method effectively solves the false causality problem caused by strong correlation and improves the accuracy of alarm propagation analysis.

Moreover, compared with structural search methods and threshold optimization methods by the coal mine process and TEP, the simplified multi-layer structure optimizes the future alarm threshold according to the probability of the alarm at the following sampling and simultaneously optimizes the false and missed alarm rates. In future research, we will optimize the estimation of alarm probability and the robustness of the adaptive optimization strategy.

References

[1] I. Izadi, S. L. Shah, D. S. Shook, T. Chen, An introduction to alarm analysis and design, IFAC Proceedings Volumes 42 (8) (2009) 645–650. `doi:http://dx.doi.org/10.3182/20090630-4-ES-2003.0386`.

[2] Y. Cheng, I. Izadi, T. Chen, Optimal alarm signal processing: Filter design and performance analysis, IEEE Transactions on Automation Science and Engineering 10 (2) (2013) 446–451. `doi:https://doi.org/10.1109/TASE.2012.2233472`.

[3] M. R. Parvez, W. Hu, T. Chen, Real-time pattern matching and ranking for early prediction of industrial alarm floods, Control Engineering Practice 120 (2022) 105004. `doi:https://doi.org/10.1016/j.conengprac.2021.105004`.

[4] M. Asaadi, I. Izadi, A. Hassanzadeh, F. Yang, Assessment of alarm systems for mixture processes and intermittent faults, Journal of Process Control 114 (2022) 120–130. `doi:https://doi.org/10.1016/j.jprocont.2022.04.002`.

[5] Q. Zhu, H. Gao, Y. Xu, A survey on alarm management for industrial processes, Acta Automatica Sinica 43 (6) (2017) 955–968. `doi:http://doi.org/10.16383/j.aas.2017.c170101`.

[6] P. Goel, E. Pistikopoulos, M. Mannan, A. Datta, A data-driven alarm and event management framework, Journal of Loss Prevention in the Process Industries 62 (2019) 103959. `doi:https://doi.org/10.1016/j.jlp.2019.103959`.

[7] V. Rodrigo, M. Chioua, T. Hagglund, M. Hollender, Causal analysis for alarm flood reduction, IFAC-PapersOnLine 49 (7) (2016) 723–728. `doi:https://doi.org/10.1016/j.ifacol.2016.07.269`.

[8] S. Lai, T. Chen, A method for pattern mining in multiple alarm flood sequences, Chemical Engineering Research and Design 117 (2017) 831–839. doi:https://doi.org/10.1016/j.cherd.2015.06.019.

[9] L. Han, H. Gao, Y. Xu, Q. Zhu, Combining fap, map and correlation analysis for multivariate alarm thresholds optimization in industrial process, Journal of Loss Prevention in the Process Industries 40 (2016) 471–478. doi:https://doi.org/10.1016/j.jlp.2016.01.022.

[10] I. Izadi, S. L. Shah, D. S. Shook, S. R. Kondaveeti, T. Chen, A framework for optimal design of alarm systems, IFAC Proceedings Volumes 42 (8) (2009) 651–656. doi:https://doi.org/10.3182/20090630-4-ES-2003.00108.

[11] J. Wang, Z. Wang, X. Zhou, F. Yang, Design of delay timers based on estimated probability mass functions of alarm durations, Journal of Process Control 110 (2022) 154–165. doi:https://doi.org/10.1016/j.jprocont.2022.01.002.

[12] N. A. Adnan, I. Izadi, T. Chen, On expected detection delays for alarm systems with deadbands and delay-timers, Journal of Process Control 21 (9) (2011) 1318–1331. doi:https://doi.org/10.1016/j.jprocont.2011.06.019.

[13] M. S. Afzal, T. Chen, Analysis and design of multimode delay-timers, Chemical Engineering Research and Design 120 (2017) 179–193. doi:https://doi.org/10.1016/j.cherd.2017.01.029.

[14] F. Yang, C. Guo, Survey on advanced alarm strategies based on multivariate analysis, in: 2017 6th International Symposium on Advanced Control of Industrial Processes (AdCONIP), IEEE, 2017, pp. 612–617. doi:https://doi.org/10.1109/ADCONIP.2017.7983850.

[15] D. Trentesaux, Distributed control of production systems, Engineering Ap-

plications of Artificial Intelligence 22 (7) (2009) 971–978. `doi:https://doi.org/10.1016/j.engappai.2009.05.001`.

[16] A. Betti, M. Tucci, E. Crisostomi, A. Piazzi, S. Barmada, D. Thomopulos, Fault prediction and early-detection in large pv power plants based on self-organizing maps, Sensors 21 (5) (2021) 1687. `doi:https://doi.org/10.3390/s21051687`.

[17] N. Zhang, X. Tian, L. Cai, X. Deng, Process fault detection based on dynamic kernel slow feature analysis, Computers & Electrical Engineering 41 (2015) 9–17. `doi:https://doi.org/10.1016/j.compeleceng.2014.11.003`.

[18] F. Yang, S. L. Shah, D. Xiao, T. Chen, Improved correlation analysis and visualization of industrial alarm data, ISA transactions 51 (4) (2012) 499–506. `doi:https://doi.org/10.1016/j.isatra.2012.03.005`.

[19] J. Cheng, J. Chen, Y.-n. Guo, S. Cheng, L. Yang, P. Zhang, Adaptive ccr-elm with variable-length brain storm optimization algorithm for class-imbalance learning, Natural computing 20 (1) (2021) 11–22. `doi:https://doi.org/10.1007/s11047-019-09735-9`.

[20] H. Gao, F. Liu, Q. Zhu, A correlation consistency based multivariate alarm thresholds optimization approach, ISA transactions 65 (2016) 37–43. `doi:https://doi.org/10.1016/j.isatra.2016.09.014`.

[21] E. Bristol, Improved process control alarm operation, ISA transactions 40 (2) (2001) 191–205. `doi:https://doi.org/10.1016/S0019-0578(00)00004-5`.

[22] M. C. van Rossum, L. B. Vlaskamp, L. M. Posthuma, M. J. Visscher, M. J. Breteler, H. J. Hermens, C. J. Kalkman, B. Preckel, Adaptive threshold-based alarm strategies for continuous vital signs monitoring, Journal of clinical monitoring and computing 36 (2) (2022) 407–417. `doi:https://doi.org/10.1007/s10877-021-00666-4`.

[23] H. Park, J. E. Choi, D. Kim, S. J. Hong, Artificial immune system for fault detection and classification of semiconductor equipment, Electronics 10 (8) (2021) 944. `doi:https://doi.org/10.3390/electronics10080944`.

[24] T.-R. Tsai, H. Xin, C.-H. Kao, Bayesian estimation based on sequential order statistics for heterogeneous baseline gompertz distributions, Mathematics 9 (2) (2021) 145. `doi:https://doi.org/10.3390/math9020145`.

[25] J. Zhu, Y. Shu, J. Zhao, F. Yang, A dynamic alarm management strategy for chemical process transitions, Journal of Loss Prevention in the Process industries 30 (2014) 207–218. `doi:https://doi.org/10.1016/j.jlp.2013.07.008`.

[26] M. T. Amin, F. Khan, S. Imtiaz, Dynamic availability assessment of safety critical systems using a dynamic bayesian network, Reliability Engineering & System Safety 178 (2018) 108–117. `doi:https://doi.org/10.1016/j.ress.2018.05.017`.

[27] Q.-Q. Meng, Q.-X. Zhu, H.-H. Gao, Y.-L. He, Y. Xu, A novel scoring function based on family transfer entropy for bayesian networks learning and its application to industrial alarm systems, Journal of Process Control 76 (2019) 122–132. `doi:https://doi.org/10.1016/j.jprocont.2019.01.013`.

[28] J. Dai, J. Ren, W. Du, V. Shikhin, J. Ma, An improved evolutionary approach-based hybrid algorithm for bayesian network structure learning in dynamic constrained search space, Neural Computing and Applications 32 (5) (2020) 1413–1434. `doi:https://doi.org/10.1007/s00521-018-3650-7`.

[29] K. Aho, D. Derryberry, T. Peterson, Model selection for ecologists: the worldviews of aic and bic, Ecology 95 (3) (2014) 631–636. `doi:https://doi.org/10.1890/13-1452.1`.

[30] A. Rodriguez, E. Ter Horst, Bayesian dynamic density estimation, Bayesian Analysis 3 (2) (2008) 339–365. `doi:https://doi.org/10.1214/08-BA313`.

[31] A. Meloni, A. Ripoli, V. Positano, L. Landini, Mutual information preconditioning improves structure learning of bayesian networks from medical databases, IEEE Transactions on Information Technology in Biomedicine 13 (6) (2009) 984–989. `doi:https://doi.org/10.1109/TITB.2009.2026273`.

[32] B.-E. Perrin, L. Ralaivola, A. Mazurie, S. Bottani, J. Mallet, F. d'Alche Buc, Gene networks inference using dynamic bayesian networks, Bioinformatics 19 (suppl_2) (2003) 138–148. `doi:https://doi.org/10.1093/bioinformatics/btg1071`.

[33] S. Yin, S. X. Ding, A. Haghani, H. Hao, P. Zhang, A comparison study of basic data-driven fault diagnosis and process monitoring methods on the benchmark tennessee eastman process, Journal of process control 22 (9) (2012) 1567–1581. `doi:https://doi.org/10.1016/j.jprocont.2012.06.009`.

[34] N. L. Ricker, Decentralized control of the tennessee eastman challenge process, Journal of process control 6 (4) (1996) 205–221. `doi:https://doi.org/10.1016/0959-1524(96)00031-5`.

[35] A. Kulkarni, V. K. Jayaraman, B. D. Kulkarni, Knowledge incorporated support vector machines to detect faults in tennessee eastman process, Computers & chemical engineering 29 (10) (2005) 2128–2133. `doi:https://doi.org/10.1016/j.compchemeng.2005.06.006`.